# Numerical bifurcation study for viscous shock and detonation waves

Blake Barker

Paris, 3 March 2015

This material is based upon work supported by the National Science Foundation under Award No. DMS-1400872. Any opinions, findings, and conclusions or recommendations expressed in this presentation are those of the author and do not necessarily reflect the views of the National Science Foundation.

# Overview

Overview of talk

- Bifurcation diagrams for various physical models
- Relation between inviscid and viscous bifurcation diagrams
- Mathematical methods needed for study
- Physical implications
- reactive Navier-Stokes
- Magnetohydrodynamics

# Motivation

(a)  (b)  (c) 

Figure: To test the effect of explosives on ships, the U.S. Navy conducted a series of experiments, called Operation Sailor Hat, on the island of Kahoolawe, Hawaii in 1965. For each test, 500 tons of TNT were stacked in 20' by 40' piles (Figure (a)) and detonated. Note the shock wave over the water in figure (b). Figure (c) shows the crater left behind. Warships typically cost on the order of a billion dollars to build.

# Motivation

Nasa is interested in developing pulsed-detonation rocket engines as they are a lightweight, low-cost alternative to traditional engines.

Figure: Pulsed-detonation powered aircraft.

# Zel'dovich-Neumann-Döring (ZND) model

Consider right-going strong detonations of the (ZND) equations

$$\begin{cases} \partial_t \tau - \partial_x u = 0, \\ \partial_t u + \partial_x p = 0, \\ \partial_t E + \partial_x (pu) = qk\phi(T)z, \\ \partial_t z = -k\phi(T)z, \end{cases}$$

with ideal gas equation of state and Arrhenius-type ignition function,

$$p = \Gamma \tau^{-1} e, \quad T = c^{-1} e,$$

$$\phi(T) = \begin{cases} \exp\left(-\mathcal{E}_A / [c_v (T - T_{\mathrm{ig}})]\right), & \text{if } T \geq T_{\mathrm{ig}} \\ 0, & \text{otherwise} \end{cases}$$

where $E = e + u^2/2$ is specific (gas-dynamical) energy, $c > 0$ is the specific heat constant, $\Gamma > 0$ is the Gruneisen constant, and $k$ and $q$ are reaction rate and heat release coefficients, and $\mathcal{E} \geq 0$ is activation energy.

# ZND spectrum

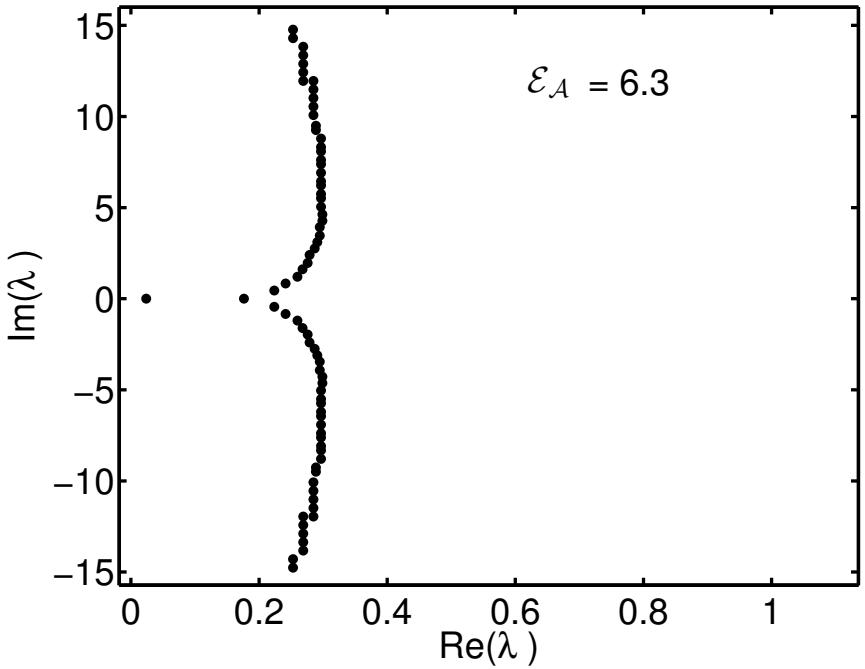


Figure: Plot of roots (0.05 relative error) of Lopatinski determinant for ZND with activation energy $\mathcal{E} = 6.3$. Roots exist outside of the viewing frame. As $\mathcal{E}$ is increased from 0, a complex conjugate pair of roots cross the imaginary axis, collide, and split. A cascade of roots continues to cross at higher frequency as $\mathcal{E}$ increases more.

# One-dimensional Hopf bifurcation

"Transition to longitudinal instability of detonation waves is generically associated with Hopf bifurcation to time-periodic galloping solutions," Benjamin Texier and Kevin Zumbrun, Comm. Math. Phys. 302 (2011), no. 1, 1-51.

- Reacting Navier-Stokes equations
- Viscous strong detonation waves
- $\forall \varepsilon$, $\lambda = 0$ is a simple root of $D(\epsilon, \cdot)$
- Transition to linear instability is generically associated with Hopf bifurcation to time-periodic galloping solutions

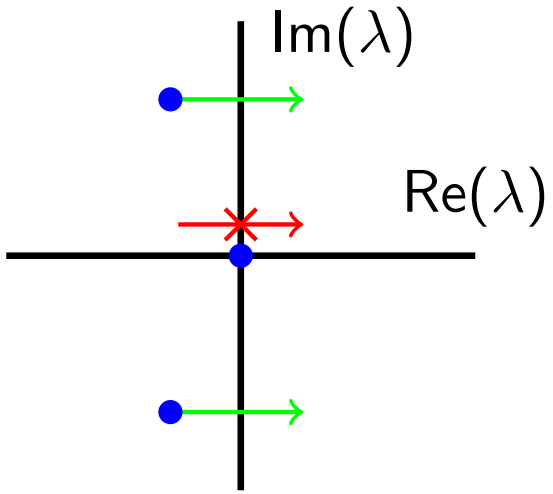

# rNS equations

The reactive Navier-Stokes (rNS) equations are given by

$$
\begin{aligned}
\tau_t - u_x &= 0\,, \\
u_t + p_x &= \left(\frac{\nu u_x}{\tau}\right)_x\,, \\
\left(e + \frac{u^2}{2}\right)_t + (pu)_x &= \left(\frac{\nu u u_x}{\tau} + \frac{\kappa T_x}{\tau}\right)_x + qk\phi(T)z\,, \\
z_t &= -k\phi(T)z + \left(\frac{Dz_x}{\tau^2}\right)_x\,.
\end{aligned}
$$

# EOS and ignition function

Ideal gas

$$p_0(\tau, T, z) = \frac{RT}{\tau}, \quad e_0(\tau, T, z) = c_v T$$

Arrhenius ignition function

$$\phi(T) = \begin{cases} \exp\left(-\mathcal{E}_A/[c_v(T - T_{\text{ig}})]\right), & \text{if } T \geq T_{\text{ig}} \\ 0, & \text{otherwise} \end{cases}$$

# Comparison of computational difficulty of rNS verse ZND

- rNS: B., Humpherys, Lyng, Zumbrun
- ZND - solve a 4 dimensional ODE with 1 growth mode per side; rNS - solve a 7 dimensional ODE with 3 growth modes per side.
- ZND - legacy study (Lee and Stewart) uses a fixed mesh; rNS- adaptive mesh
- rNS: use the well-conditioned polar coordinate method of Humpherys and Zumbrun.
- Example - parameters: $\nu = 0.1$, $T_{\text{ig}} = 0.99$, $\Gamma = 0.2$, $q = 0.623$, $e_+ = 0.062$, and $\mathcal{E}_A = 5$
- rNS profile: 4.77 seconds, ZND profile: 1.69 seconds
- Root solve on shifted unit square - rNS: 13.7 minutes, ZND: 24.7 seconds
- For $\mathcal{E}_A = 4$, ZND Lopatinski determinat: $R = 4$, time $= 16.9$ seconds, roots $= 14$; rNS Evans function: $R = 64$, time $= 65.4$ seconds, roots $= 2$.

# Eigenvalues of rNS

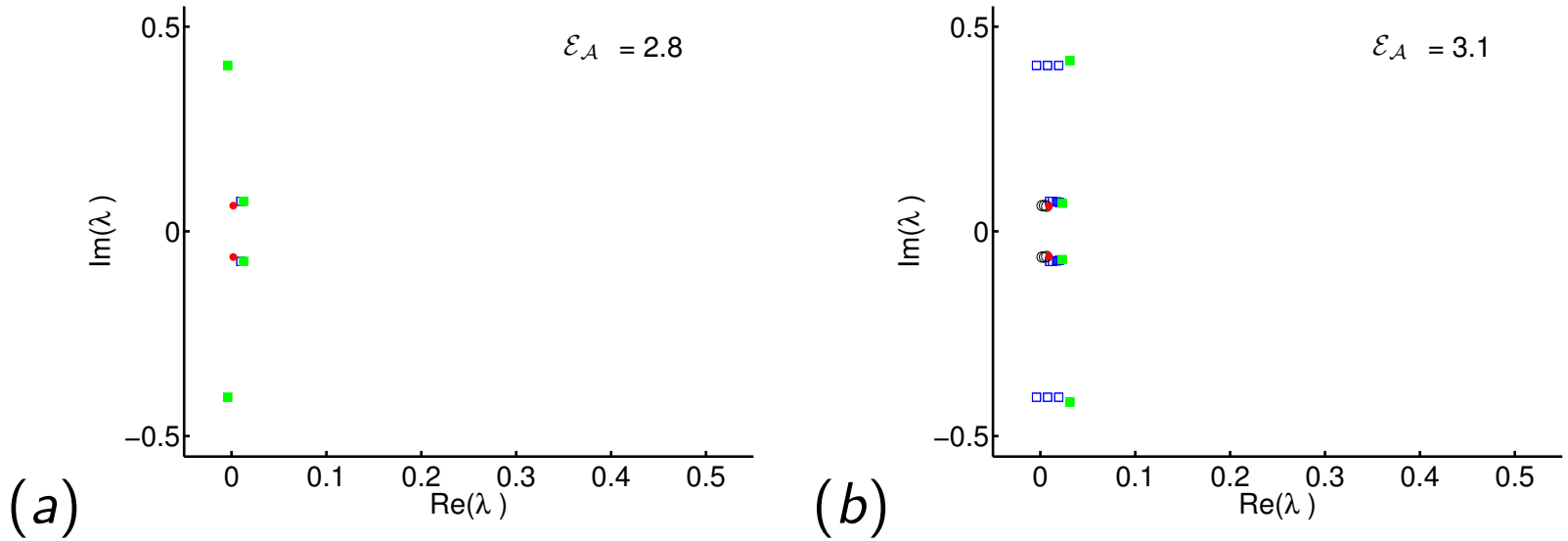


Figure: The movement of unstable roots in the complex plane as $\mathcal{E}_A$ increases. Circles (solid dot for current value of $\mathcal{E}_A$, open circles for previous values) mark the roots corresponding to the RNS model, while open squares (solid square for the current value of $\mathcal{E}_A$, open squares for previous values) correspond to the ZND model. The smaller modulus roots enter for $\mathcal{E}_A \approx 2.75$ (Panel (a))

# Eigenvalues of rNS

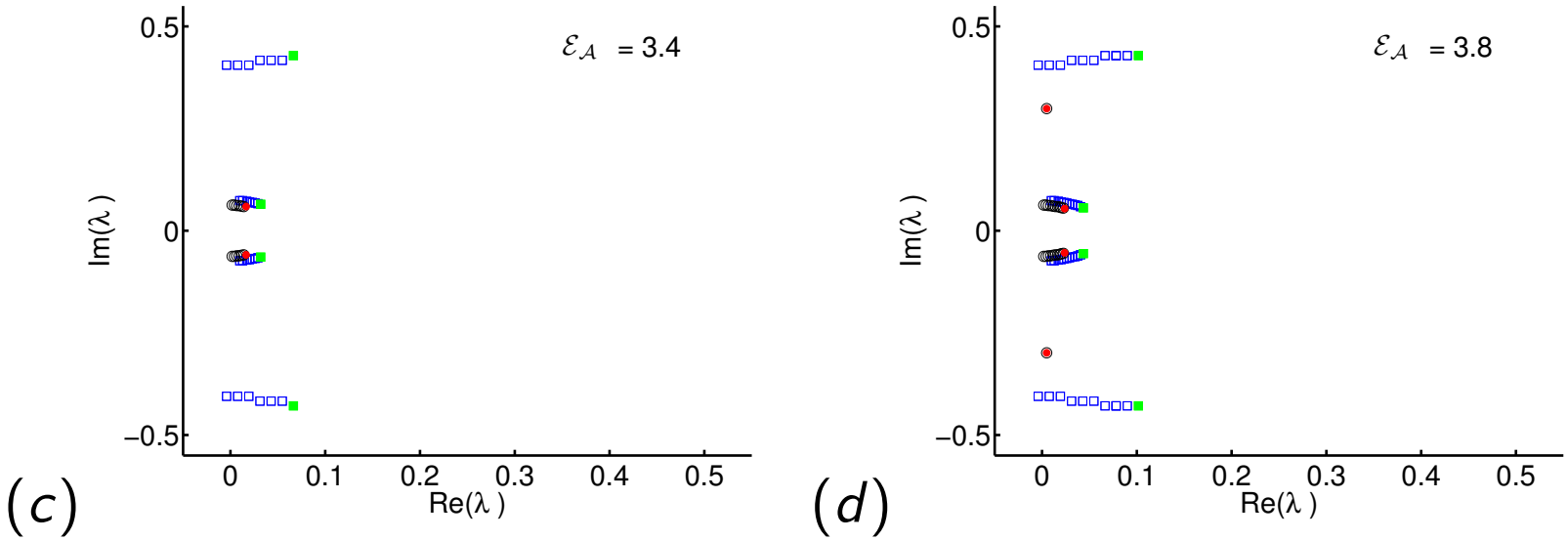

# Eigenvalues of rNS

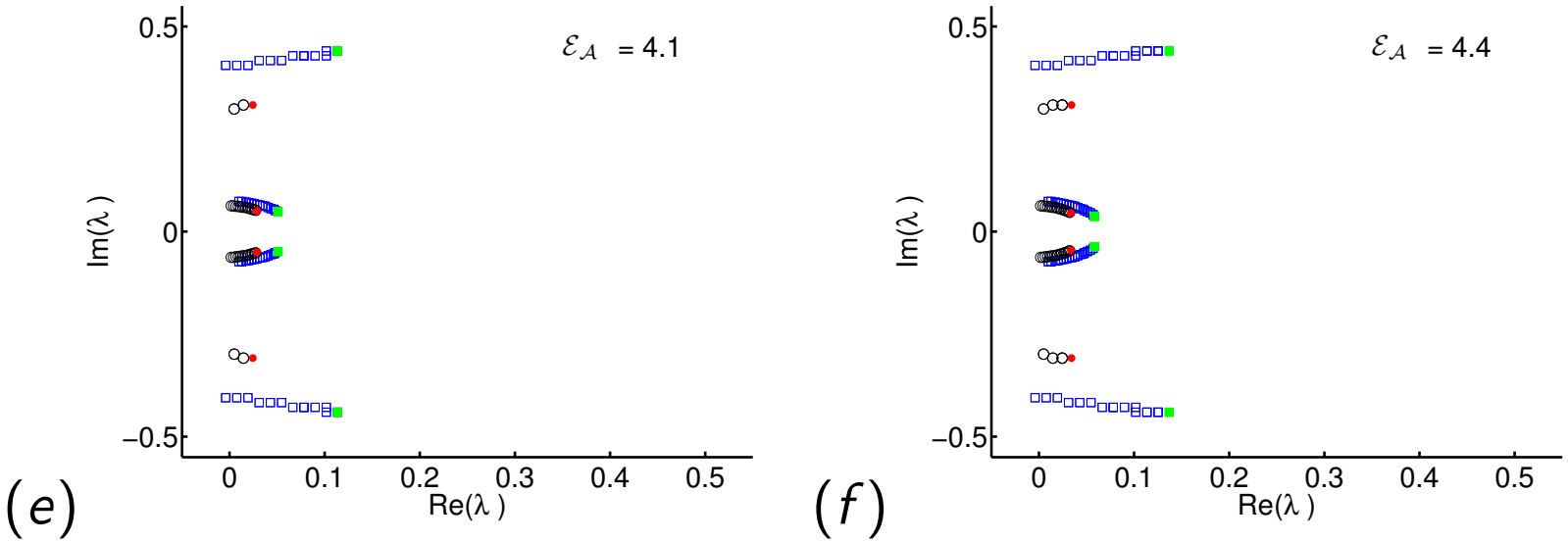

# Eigenvalues of rNS

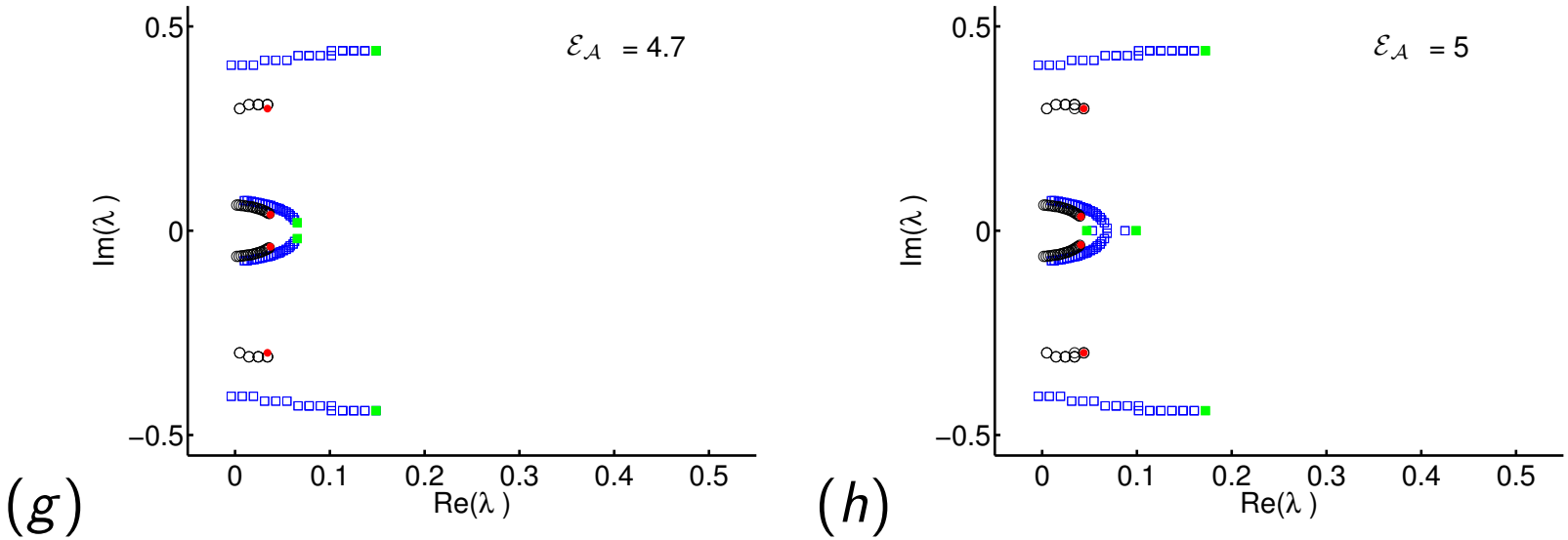


(g) (h)

# Eigenvalues of rNS

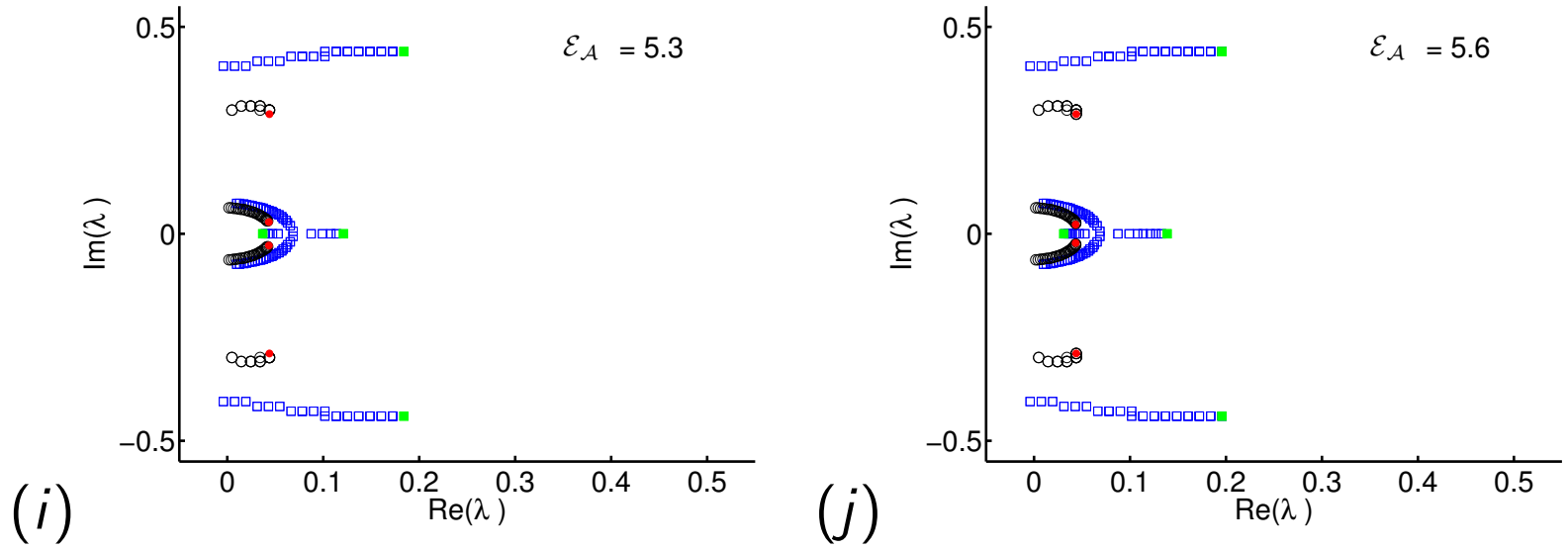


Figure: The high modulus roots have a turning point at about $\mathcal{E}_A \approx 5.2$, and the smaller modulus roots have theirs at $\mathcal{E}_A \approx 5.5$.

# Eigenvalues of rNS

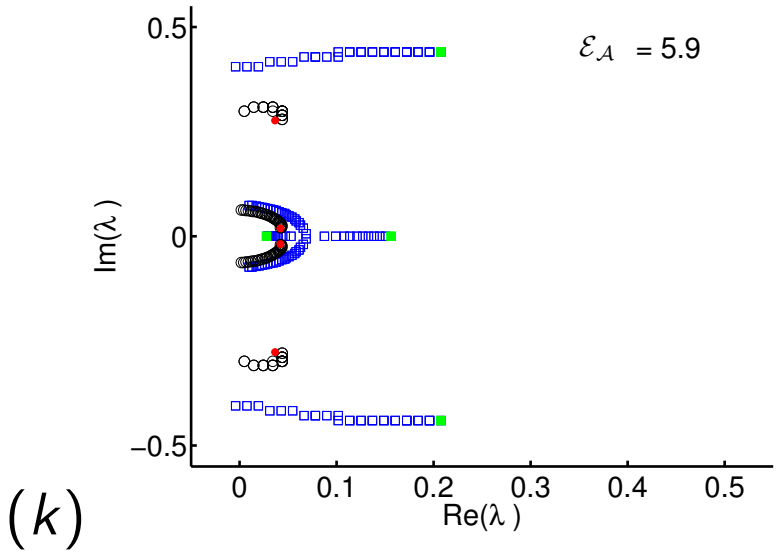


(k)

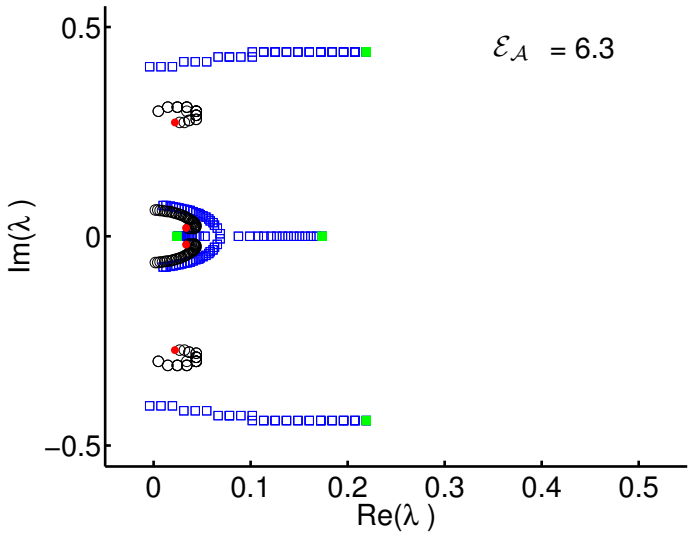


(l)

# Eigenvalues of rNS

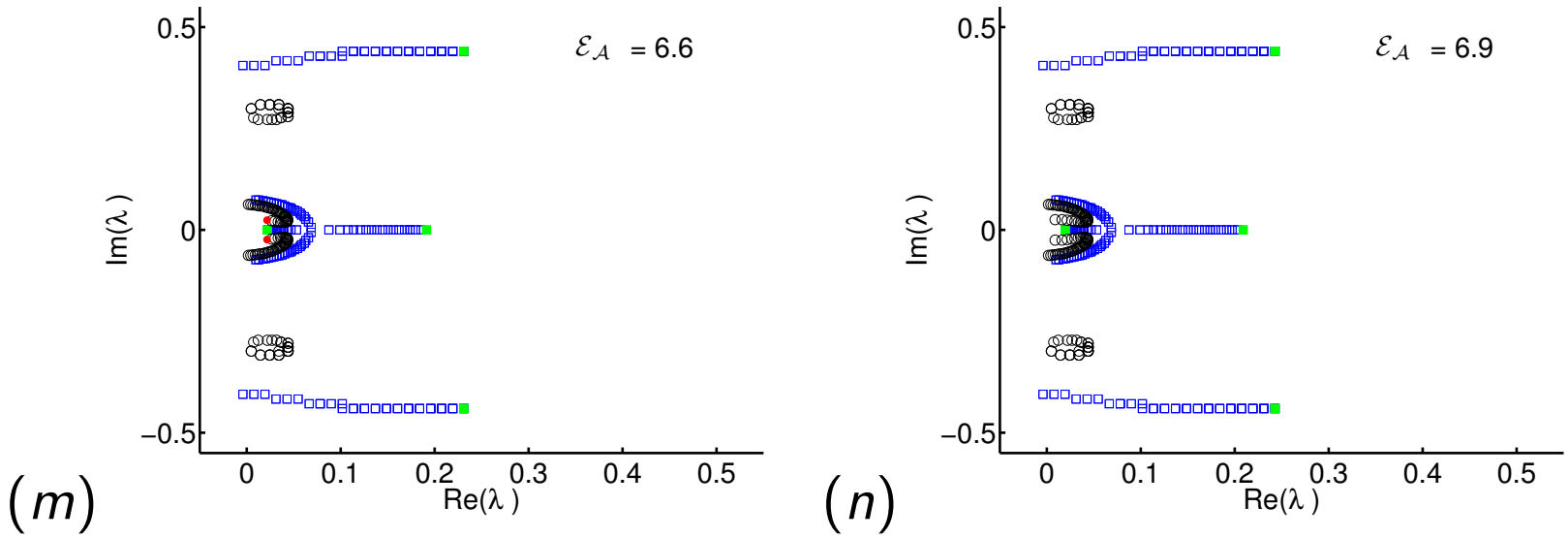


(*m*) (*n*)

Figure: The large modulus roots leave at $\mathcal{E}_A \approx 6.55$ and the small modulus roots leave at approximately $\mathcal{E}_A \approx 6.85$ (Panel (n)).

# Neutral stability boundaries in the $\mathcal{E}_A$-$\nu$ plane

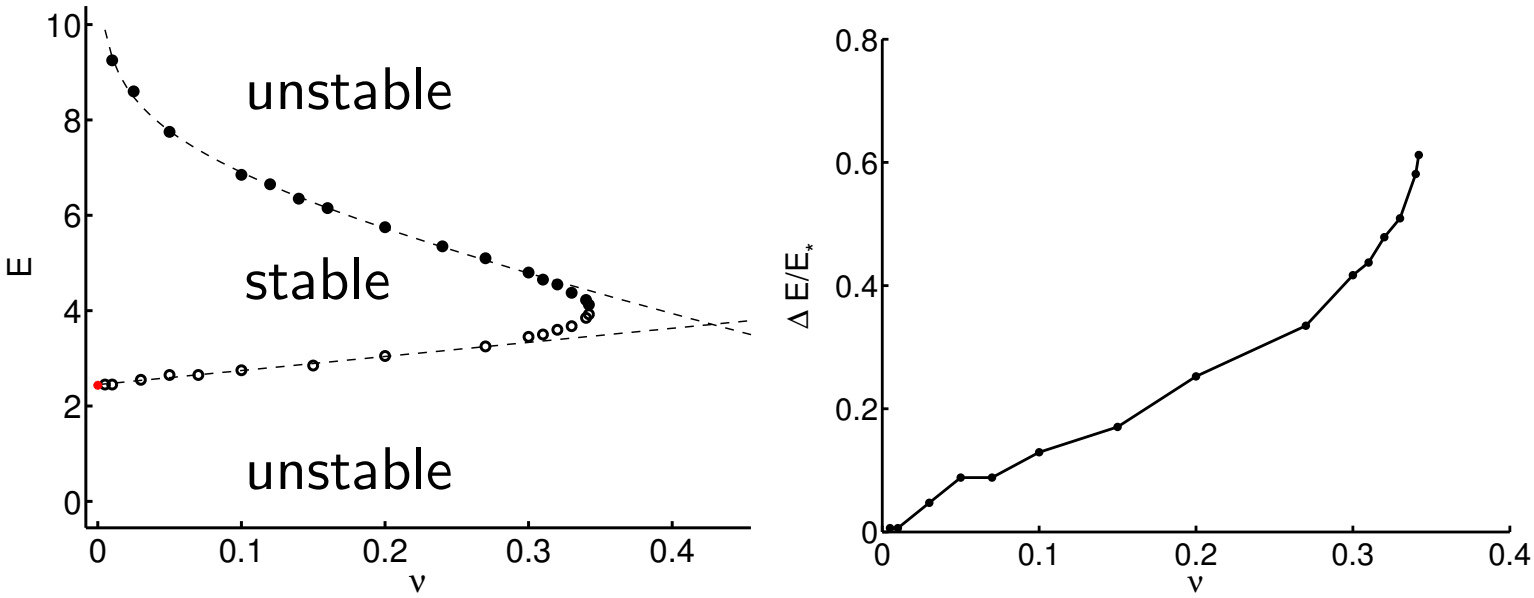


Figure: LEFT: Neutral Stability Boundaries in the $\mathcal{E}_A$-$\nu$ plane. The upper and lower stability boundaries ($\mathcal{E}_A^{\pm}$) are denoted by black dots and circles, respectively; the red dot denotes the ZND (inviscid) stability boundary. The best-fit curve (dashed line, $\nu < 0.27$) for the upper boundary is $\mathcal{E}_A^{+}(\nu) = 5.67 - 6.16\nu - 0.804\ln(\nu)$. For the lower boundary, the best-fit curve (dashed line, $\nu \leq 0.27$) is linear: $\mathcal{E}_A^{-}(\nu) = 2.45 + 2.95\nu$. Here, $\nu = d = \kappa$, $\Gamma = 0.2$, $e_+ = 6.23\text{e-}2$, $q = 6.23\text{e-}1$, and $T_{\text{ig}} = 0.99$. RIGHT: Viscous Delay: We plot $\Delta E/\mathcal{E}_* = (\mathcal{E}_A^{-}(\nu) - \mathcal{E}_*)/\mathcal{E}_*$ against $\nu$, where $\mathcal{E}_*$ is the approximation to the ZND neutral boundary. Here, $\nu = D = \kappa$, $\Gamma = 0.2$, $e_+ = 6.23\text{e-}2$, $q = 6.23\text{e-}1$, and $T_{\text{ig}} = 0.99$.

# Motivation: Magnetohydrodynamics (MHD)

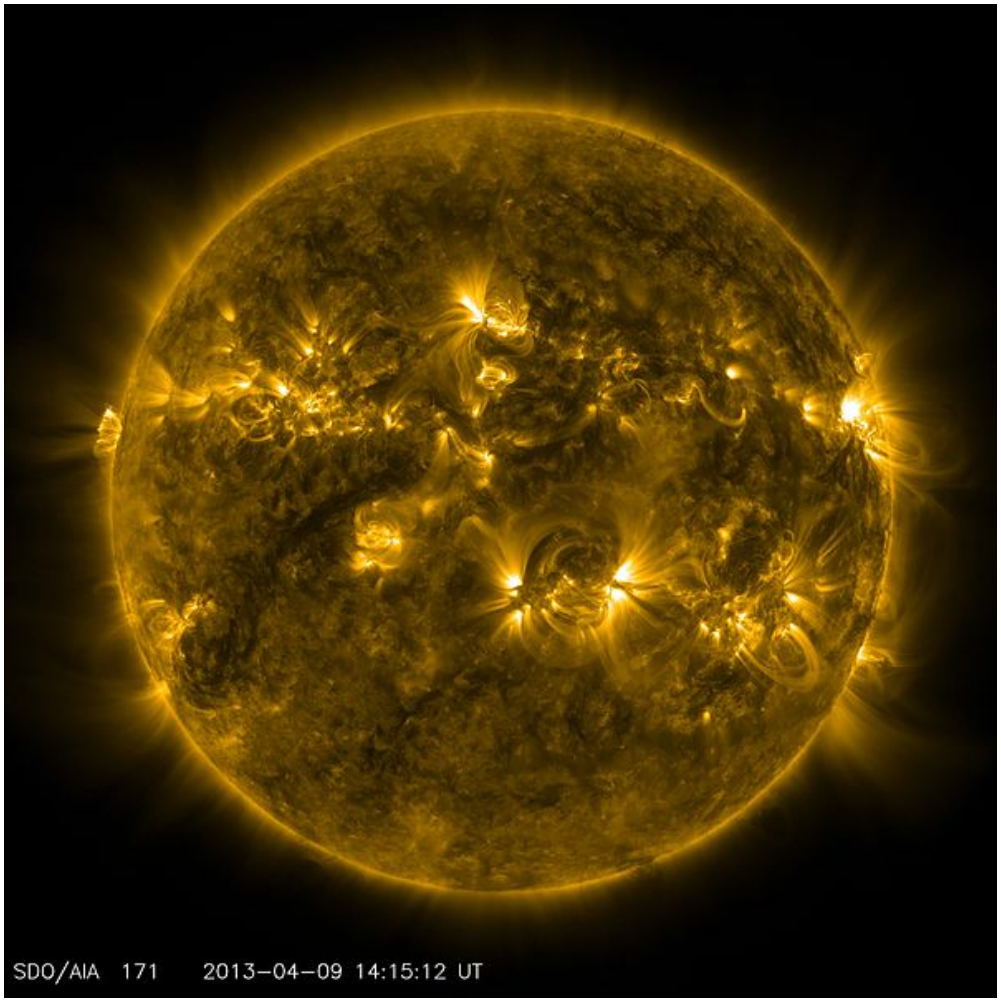


Figure: NASA picture of our sun.

# MHD equations in multi-d

The inviscid MHD equations are given by

$$\begin{aligned}
\rho_t + \operatorname{div}(\rho u) &= 0, \\
(\rho u)_t + \operatorname{div}(\rho u \otimes u - H \otimes H) + \nabla q &= 0, \\
H_t - \nabla \times (u \times H) + \alpha \operatorname{div}(H) e_1 &= 0, \\
(E + H^2/2)_t + \operatorname{div}((E+p)u + H \times (u \times H)) &= 0,
\end{aligned}$$

and the viscous MHD equations by

$$\begin{aligned}
\rho_t + \operatorname{div}(\rho u) &= 0 \\
(\rho u)_t + \operatorname{div}(\rho u \otimes u - H \otimes H) + \nabla q &= \mu \Delta u + (\mu + \eta) \nabla \operatorname{div} u \\
H_t - \nabla \times (u \times H) + \alpha \operatorname{div}(H) e_1 &= \nu \Delta H \\
(E + H^2/2)_t + \operatorname{div}((E+p)u + H \times (u \times H)) &= \operatorname{div}(\Sigma u) + \kappa \Delta T + \nu \operatorname{div}(H \times (\nabla \times H)),
\end{aligned}$$

along with the divergence free condition $\operatorname{div}(H) = 0$. Note the addition of the $\alpha$ term.

# Two-dimensional Hopf bifurcation in a channel

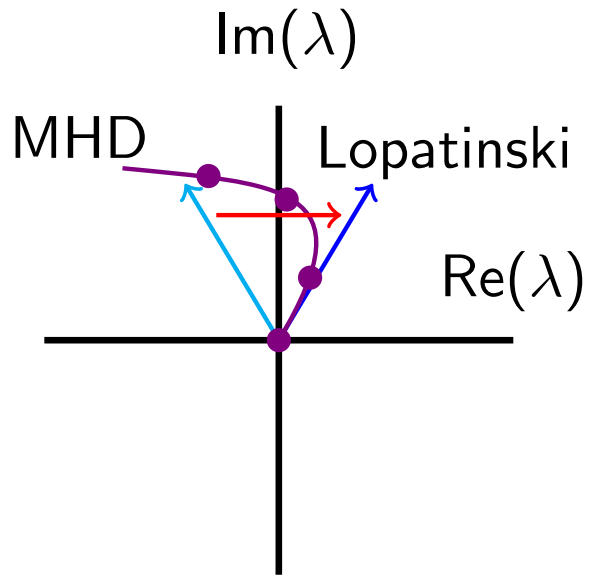


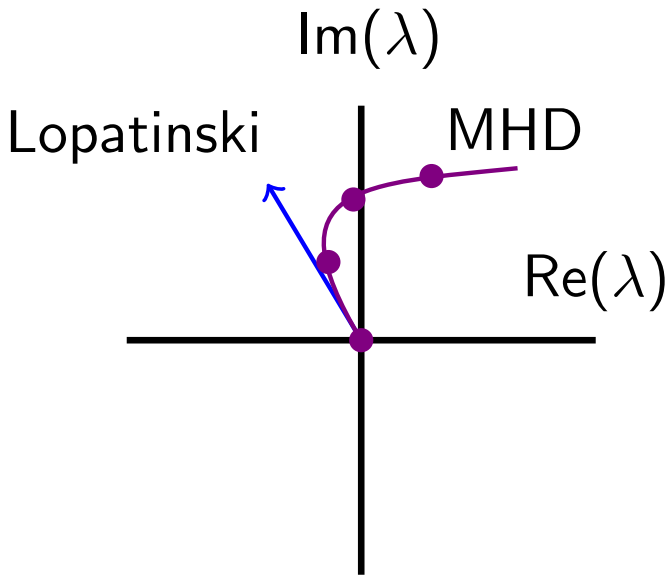


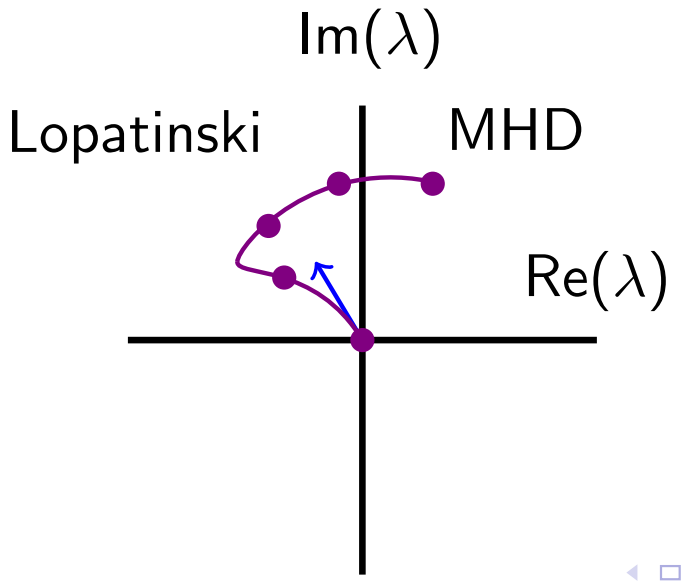

# Pseudo-Lagrangian coordinates

The isentropic Navier–Stokes equations in Eulerian coordinates in one space dimension with viscosity coefficient set to 1 are

$$\rho_t + (\rho u)_x = 0\,,$$
$$(\rho u)_t + (\rho u^2 + p(\rho))_x = u_{xx}\,.$$

Make coordinate change

$$y(x,t) = \int_{x^*(t)}^{x} \rho(z,t)\,\mathrm{d}z,$$
$$\frac{\mathrm{d}x^*}{\mathrm{d}t} = u(x^*(t),t), \quad x^*(0) = 0.$$

# Pseudo-Lagrangian coordinates

Observe that

$$\frac{\partial y}{\partial x}(x,t) = \rho(x,t)\,,$$

and

$$\begin{aligned}
\frac{\partial y}{\partial t}(x,t) &= \int_{x^*(t)}^{x} \frac{\partial \rho}{\partial t}(z,t)\,\mathrm{d}z - \rho(x^*(t),t)\frac{\mathrm{d}x^*}{\mathrm{d}t} \\
&= -\int_{x^*(t)}^{x} \partial_z(\rho u)\,\mathrm{d}z - \rho(x^*(t),t)u(x^*(t),t) \\
&= -\rho(x,t)u(x,t) + \rho(x^*(t),t)u(x^*(t),t) \\
&\quad - \rho(x^*(t),t)u(x^*(t),t) \\
&= -\rho u(x,t)\,.
\end{aligned}$$

# Pseudo-Lagrangian coordinates

Thus, defining

$$\tau(y(x,t),t) = \frac{1}{\rho(x,t)}, \quad w(y(x,t),t) = u(x,t)$$

and, denoting by $P$ the pressure as a function of specific volume, we find that the Lagrangian formulation of of isentropicgas is

$$\tau_t - w_y = 0,$$
$$w_t + P(\tau)_y = \left(\frac{w_y}{\tau}\right)_y.$$

See texts of Courant & Friedrichs or Serre for further information about this coordinate change.

# Pseudo-Lagrangian verse Lagrangian coordinates

Evans function asymptotic behavior: $e^{C\sqrt{\lambda}}$ verse $e^{C\lambda}$

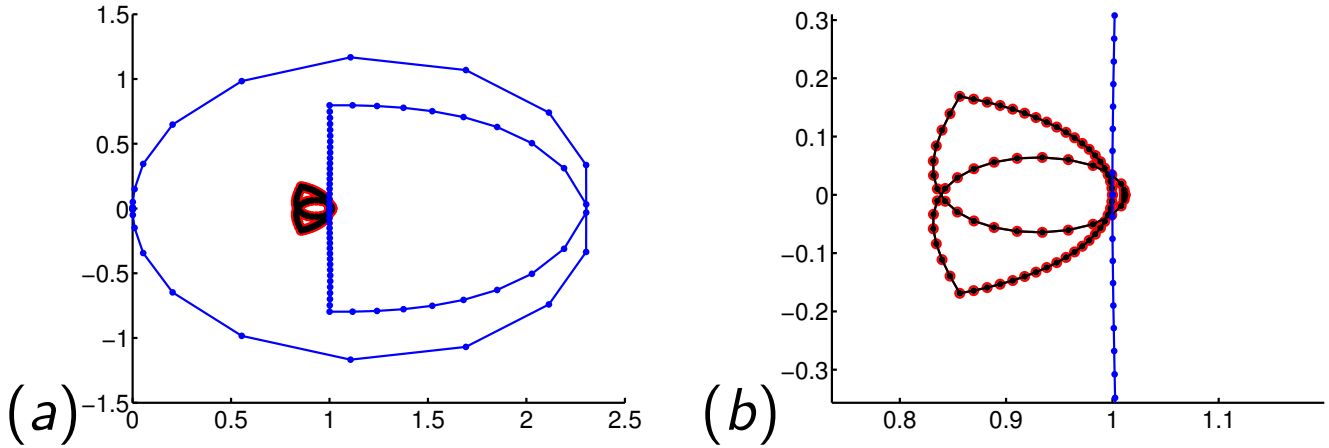


Figure: Plot of the Evans function for isentropic gas in 1d ($\gamma = 5/3$, $u_{1+} = 0.3$) computed on a semicircular contour of radius $R = 10$ using the polar coordinate method and the adjoint formulation on the right. (a) Plot of the Evans function in Eulerian coordinates (blue), Lagrangian coordinates (black), and pseudo-Lagrangian coordinates (red). (b) A zoom in of Figure (a).

# Multi-d Evans function computation

- First planar multi-d study is gas: HLyZ
- This is first planar multi-d study of MHD
- Evans function ODE set up with symbolic code
- Planar multi-d Evans function now supported in STABLAB

# MHD: Numerical verification that root is simple

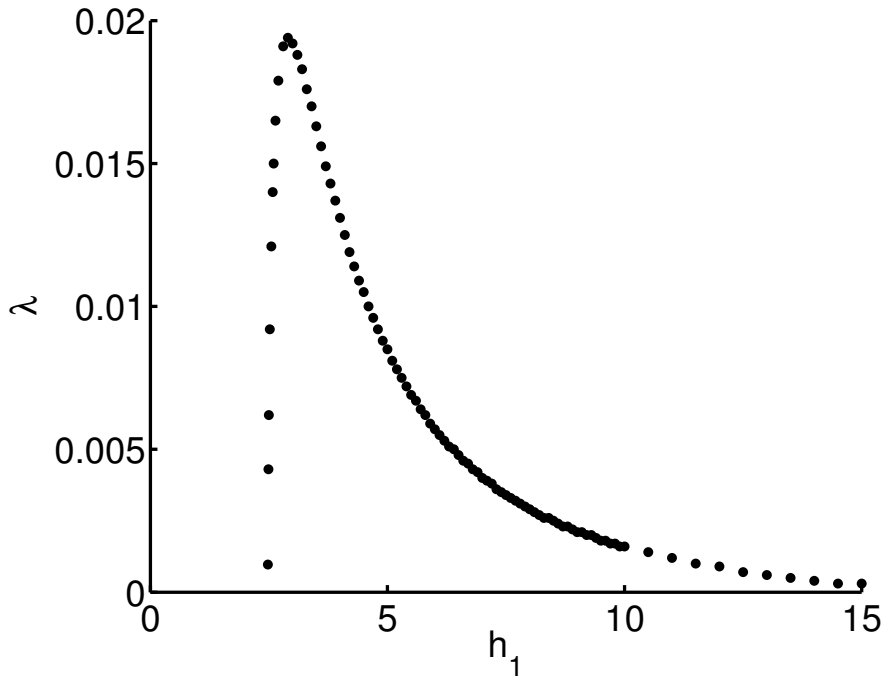


Figure: Plot of the roots of the Lopatinski determinant against $h_1^*$ for $\xi = 1$ and $\gamma = 5/3$, $u_{1+} = 0.9$.

# Isentropic MHD inviscid stability diagram (Lopatinski)

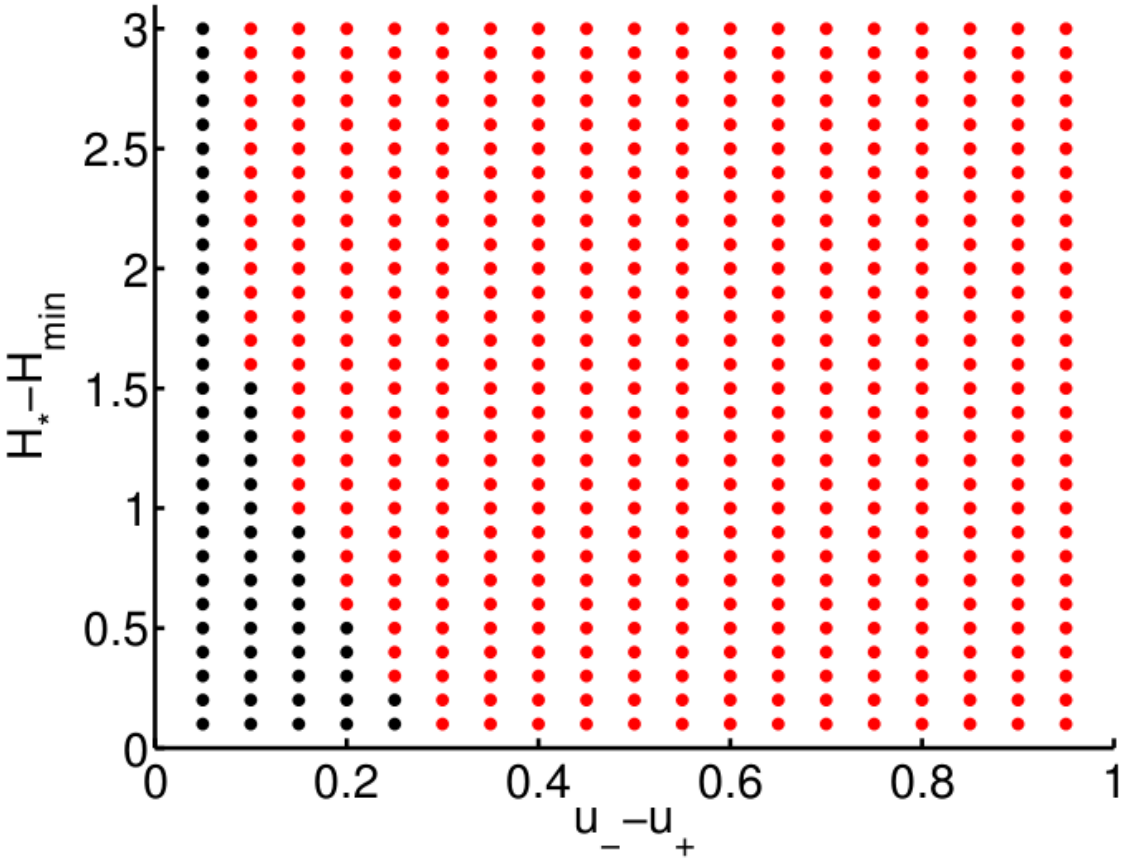


Figure: Plot of inviscid stability diagram for $\gamma = 5/3$. Black corresponds to stability and red to instability.

# Roots of the Evans function for isentropic MHD

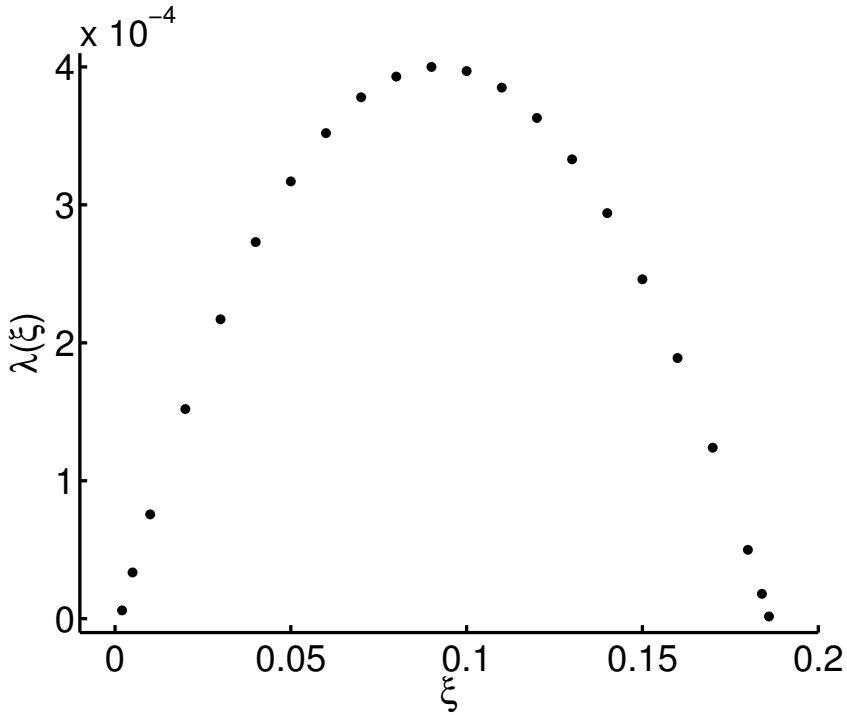


Figure: Plot of $\lambda(\xi)$ against $\xi$ where $D(\lambda(\xi), \xi) = 0$ for $h_1 = 3$, $\gamma = 5/3$, $u_{1+} = 0.6$, $\mu = \nu = \kappa = 0.1$, $\eta = -0.067$, $\alpha = 1$.

# Eigenfunction for isentropic MHD superimposed on wave

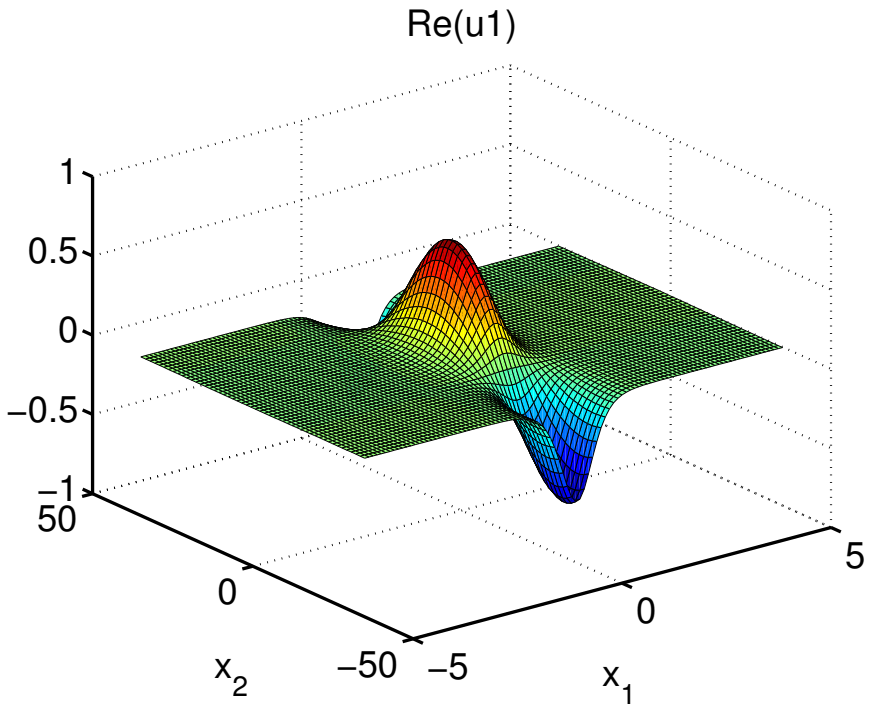


Figure: Plot of the real part of the $u_1$ component of the Eigenfunction superimposed on background wave solution to approximate the nonlinear solution for $h_1 = 3$, $\gamma = 5/3$, $u_{1+} = 0.6$, $\nu = \mu = \kappa = 0.1$, $\eta = -0.067$.

# Summary and open questions

Summary

- Beyond stability to physical behavior
- Use the mathematical model to provide data
- We can do multi-d Evans function computations now for the first time, and we have already seen interesting phenomena (something not in 1d) and we expect to see more.

Open question

- Are there systems where viscous instability precedes inviscid instability as shock amplitude is increased from 0 (stable)?